

COMPARISON OF THE DEGREE OF INFLUENCE OF VARIOUS CONDITIONS ON THE BEARING CAPACITY OF WOOD-BASED PANELS

Ryutaro Sudo¹, Kenji Aoki¹,

ABSTRACT: Bearing property is important for the design of the connection. There are few studies about the bearing property of the wood-based panels. First, the tensile bearing test of the wood-based panels: Plywood and OSB of strong and weak axial specification, was conducted based on the comprehensive parameters. Test parameters were set as dowel insertion position, size of pilot hole and dowel diameter. The correlation between parameters and the mechanical characteristics: failure behavior, ductility, yield stress and maximum stress, was verified. To verify how much each parameter effect on maximum stress, standardized multiple regression analysis was conducted. These results provide insights into the failure behavior and stress distribution, supporting certain assumptions: (1) PW and OSB is deformed dominantly in-plane and out-of-plane respectively; (2) the relative stress spread range is decreased with the larger diameter of the dowel; (3) the stress spread range is widened by load step; and (4) the bearing stress is spread vertically and horizontally in strong and weak specification respectively, also verified in this section. A detailed investigation was performed using DIC and CT scanning techniques to shed light on the stress distribution and fracture processes. Three load steps were configured and subjected to cyclic loading. Verification and comparison were carried out for each specification, layer, and step, providing a clearer understanding of the stress distribution and fracture processes. These results are consistent with the conclusions drawn from the comprehensive testing.

KEYWORDS: Bearing, Wood-based panel, Plywood, OSB, Standardized multiple regression analysis, DIC, CT scan

1 INTRODUCTION

The structural properties of wood structures are greatly affected by the property of joints. Their behavior depends on the characteristics when the circular joints are embedding into the material, the bearing properties. There have been many studies on the bearing properties of timber¹⁾²⁾. On the other hand, though studies on the bearing capacity of wood-based panels include Sekino et al.'s study on particle board³⁾ and Ogawa et al.'s study on the bearing capacity of plywood⁴⁾, there are only a few studies that have comprehensively examined the parameters and considered how the various conditions affect the bearing properties and how the degree of influence varies depending on the type of panels. The underlying mechanism of fracture remains elusive, which represents a crucial foundation for the development of theoretical equations for determining characteristic values.

The primary objective of this report is to systematically investigate the degree to which various conditions exert an influence on mechanical properties under the bearing stress of plywood (PW) and oriented strand board (OSB) through comprehensive testing. Additionally, the process of stress spread, and fracture was clarified by utilizing

digital image correlation (DIC) and computed tomography (CT) scanning techniques.

2 STUDY BASED ON EXHAUSTIVE PARAMETERS

2.1 Material and method

The panels to be tested were 5-ply cedar PW⁵⁾ and OSB⁶⁾ for structural use. Since PW and OSB were orthotropy material, the test was conducted in both strong and weak axes. In addition, a trailing “-s” (e.g., PW-s) indicates a strong axial specification, whereas a trailing “-w” (e.g., PW-w) indicates a weak axial specification. Their thickness was 9mm.

The detail properties of the panels are shown in Table 1. Other parameters were set as dowel diameter d (5.2 and 12mm), position (A~G), as shown in Figure

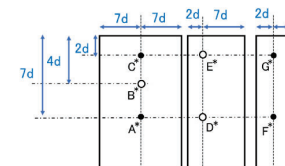


Figure 1: Parameters of bearing tests. * Name of Position. Tests of 4 kinds of ph were conducted at place of black circle. Tests of 2 kinds of ph (0, 1d) were conducted at place of white circle.

¹ Ryutaro Sudo, Japan. Department of Biomaterials Sciences, Graduate School of Agricultural and Life Sciences, The University of Tokyo, 1-1-1
sudo-ryutaro282@g.ecc.u-tokyo.ac.jp

Kenji Aoki, The University of Tokyo, Japan.
aoken@g.ecc.u-tokyo.ac.jp

1, the size of the pilot hole ph (0, 1/3, 2/3 and 1 time to the diameter). Figure 1 also shows the combination of the position and ph . As a dowel ($d=5.2\text{mm}$),



Figure 2: Schematic of 12mm pin.

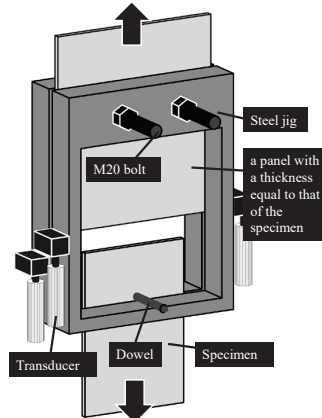


Figure 3: Setting of bearing test.

N150 nail (defined by JIS⁷⁾) was used and, as the other dowel ($d=12\text{mm}$), a custom-made dowel was used, as shown in Figure 2. Number of the specimen were six per a specification. Bearing test was conducted as shown in Figure 3, applying shear force by sandwiching with a pair of steel plates with a rectangular hole. This jig was designed to enable to observe of the failure process and to eliminate depth clearance. The monotonical tensile load was applied to the specimen at 3~4mm/min ($d=5.2\text{mm}$) or at 6~7mm/min ($d=12\text{mm}$). After the test, bending deformation of the dowel was not observed.

2.2 RESULT AND DISCUSSION

2.2.1 Failure mode

Two failure modes were observed as follows. One was shear failure at the area above dowel, as shown in Figure 4. It was named as “ESF (end shear failure)”. The Other was tensile failure at the area next to the dowel, as shown in Figure 5. It was named as “STF (Side tension failure)”. ESF was ductile failure, whereas STF was brittle failure. STF occurred only when the dowel position was D~G. The STF resembled a simple tensile failure, and it did



Figure 4: The photo of ESF.

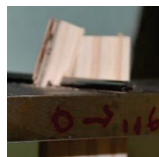


Figure 5: The photo of STF.

Table 1: Fundamental properties of wood-based structural panels.

		Density (kg/m ³)	MC (%)	In-plane		Internal board		In-plane		Other information
				Strength (MPa)	Elastic modulus (GPa)	Strength (MPa)	Elastic modulus (GPa)	Strength (MPa)	Elastic modulus (GPa)	
PW	Ave.	416	11.1	13.5	5.28	0.930	0.0151	4.72	0.619	wood species; Cryptomeria japonica (Japanese cedar) Number of layers; 5, class; 2nd, use; for structural use [5].
	S. D.	20	1.2	4.0	1.56	0.245	0.0089	0.14	0.095	
OSB	Ave.	635	7.7	16.3	6.85	0.477	0.0098	9.97	1.838	Number of layers; 3, class; 4th [6].
	S. D.	42	0.7	4.1	0.96	0.147	0.0063	1.25	0.433	

Note: Ave. means average, and S. D. means standard deviation. Three mechanical tests were conducted according to ASTM D 1037 [8].

not differ significantly among the panel types. Meanwhile, the ESF showed some differences among the panel types. Figure 6 shows a summary of the fracture progression during the test and the failure appearance of each panel after the test. In this figure, all parameters

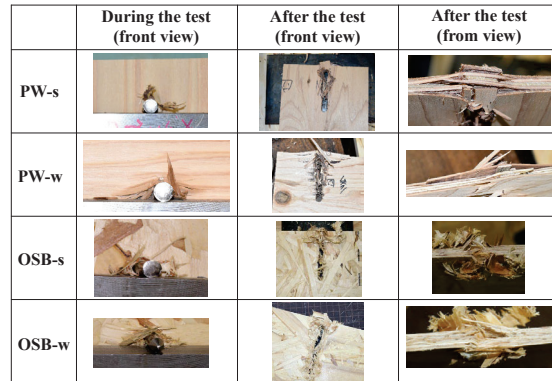


Figure 6: Comparison of ESF behavior among panel types.

except the panel type are standardized uniformed (dowel position: A, d : 12 mm, ph : 1).

The ESF mode exhibited two types of failure behavior: a crack on the surface of the panel generated by in-plane tensile or shear stress, termed “in-plane failure,” and a peeled surface divided into several layers. The peeled surface failure is generated by the Poisson effect of the compressive stress immediately above the dowel and is termed “out-of-plane failure.”

Although these two types of failure behavior generally occurred simultaneously, it was possible to identify the dominant failure behavior for each panel type.

After the test was completed, vertical and horizontal crack lines were observed in PW-s and PW-w, respectively. Although the layers of the specimens were separated after the test, they were only slightly peeled off. This separation of layers was caused by the difference in failure mode in the fiber direction of the veneer, not by the Poisson effect. Compared with the PW, the OSB did not show a clear crack line. Additionally, the surface layer of the OSB was peeled off more significantly than that of the PW. Therefore, based on a comparison between the PW and OSB, in-plane failure and out-of-plane failure were dominant in the PW and OSB, respectively.

To correlate these failure behaviors with the material property, the “in-to-out plane strength,” which is defined by the tensile strength divided by the internal bond strength, was introduced. The in-to-out plane strengths of the PW and OSB were 14.6 and 34.6 respectively. A comparison of the in-to-out plane strength of panels shows that a panel with a higher in-to-out plane strength is dominated by the out-to-plane failure. The fracture mechanism is shown in Figure 7. These results suggests that the in-to-out plane strength is related to the failure behavior under the bearing pressure.

Number of specimens where STF occurred at D~G is shown in Table 2. About all of panels, STF more likely

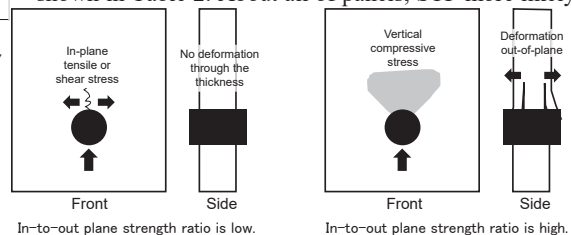


Figure 7: Two fracture processes of ESF.

Table 2: Number of specimens where STF occurred.

The dowel position	ph	PW-s		PW-w		OSB-s		OSB-w	
		d=5.2	d=12	d=5.2	d=12	d=5.2	d=12	d=5.2	d=12
D	0	3	2	5	3	3	2	5	4
	1	4	1	5	2	5	1	6	5
E	0	3	3	5	4	1	1	4	3
	1	4	0	5	4	1	2	2	3
F	0	3	3	6	0	6	4	6	5
	1/3	4	2	6	5	6	3	6	6
	2/3	5	2	6	4	4	3	6	6
	1	4	0	6	5	6	5	6	6
G	0	3	4	5	4	6	2	5	5
	1/3	3	2	5	4	5	3	5	6
	2/3	1	1	5	4	5	2	6	5
	1	2	0	3	3	6	0	6	4

occurred at the position of D and F than of E and G respectively. It is considered to be because ESF occurred earlier than STF when edge distance was short. This Table also indicates that STF more likely occurred when d was 5.2mm than when 12mm. According to some previous studies about embedment of timber⁹), stress spreading range is absolute range: not depending on the pressure area. Configuring the length of edge distance based on the diameter in this test, stress spreading range was wider relatively with $d = 5.2\text{mm}$ than $d = 12\text{mm}$. Assuming that STF occurred when strong stress reached to the edge of specimen, this difference of the range is considered to result in the difference of the number of specimen where STF occurred. STF also more likely occurred loading in weak axis than in strong axis. This result suggests that horizontal stress spread range of weak axial specification was wider than that of strong one. Compared in the two kinds of panels, STF occurred more likely in OSB.

2.2.2 Evaluation method of characteristic value

Stress was calculated by dividing the load by the projection area of the dowel, after which the stress–displacement curves were obtained. Based on these displacement curves, the maximum stress σ_{\max} (MPa), yield stress σ_y (MPa), and ultimate displacement u (mm) were derived using the method presented next.

A simple illustration of the method is shown in Figure 8. u was defined as the displacement at 80% of the maximum stress of the entire stress–displacement curve. σ_y was derived via the 5%-offset method using a linear elastic line in the linear range (i.e., offset the length to equal to 5% of the dowel diameter). Additionally, based on the cases where STF occurred, STF was shown to be

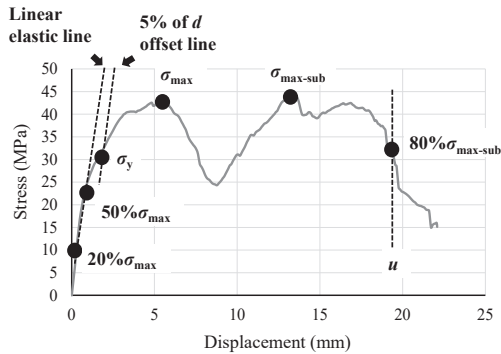


Figure 8: Evaluation of characteristic values based on stress–displacement curve. Note: The parameters of the specimen were as follows: panel type, PW-s; d , 5.2 mm; ph , 0; dowel position, A.

a brittle failure, and the intersection between its curve and

the offset line typically occurred after σ_{\max} . In this case, σ_{\max} was regarded as σ_y .

2.2.3 Comparison of ductility

The ultimate displacement is typically used to compare ductility. However, as the ultimate displacement measured in this study was significantly affected by the original end distance, it was not regarded as an appropriate indicator of ductility. Additionally, the original end distance was set based on d , and u is also affected by d . Hence, the remaining distance (RD) was introduced, which is derived by dividing the difference between u and the length of the original end distance by d . Figure 9 shows a comparison of the RD values. The shorter the RD , the higher is the ductility.

The trends observed in all the panel types were as follows: (1) The RD of A and B was similar, (2) the RD at D or F and their standard deviations were higher than those at any other dowel positions, and (3) the RD for $d = 5.2$ mm was typically higher than that for $d = 12$ mm.

First, the RD of A and B was similar, i.e., from 2 to 4. For the bearing of timber, if the ratio of the thickness to d is low and dowel bending is not observed, then brittle splitting will typically occur. For the bearing of wood-based panels, when the edge distance was sufficient, the failure mode was ductile, and the load did not decrease until the remaining end distance reached a certain value. This implies that the prevalent belief for timber is not valid for wood-based structural panels. This mechanism is independent of the original end distance.

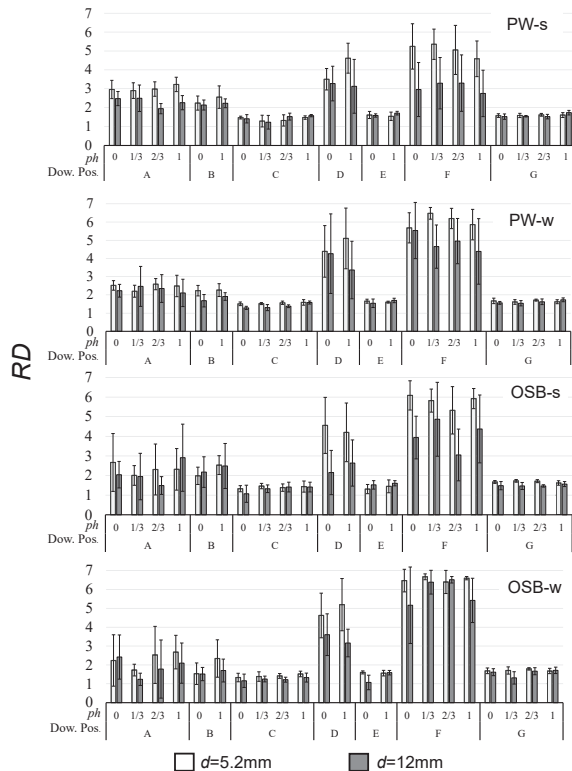


Figure 9: Comparison of RD values. Note: Dow. Pos. means dowel position. Error bars indicate standard deviation.

Second, the values of RD at D or F and their standard deviations were higher than those at any other dowel positions. As described previously, the failure mode at dowel position D or F was STF in some cases and brittle. Consequently, the values of RD at D and F were high. In addition, a mixture of failures involving both ESF and STF occurred in the same specification, which resulted in a significant variation in the RD .

Third, the RD for $d = 5.2$ mm was higher than that for $d = 12$ mm. As described above, the spreading range of the horizontal stress was assumed to be larger when $d = 5.2$ mm in comparison with $d = 12$ mm. Therefore, the results at positions D–G, where STF is likely, can be theorized as in the previous section. Although ESF occurred at dowel positions A–C, the same justification can be used to explain these results, assuming the spreading range of the longitudinal relative stress was also larger when $d = 5.2$ mm. Therefore, this suggests that the relative stress spreading range was larger both horizontally and vertically when $d = 5.2$ mm in comparison with $d = 12$ mm.

A comparison of the RD values based on calculated “strong axial specification - weak axial specification” values for the PW and OSB are shown in Figure 10.

The values were positive at positions A–C and negative at positions D and F for both the PW and OSB. In the weak axial specification, STF occurred more frequently, and the RD was higher, as described above. Therefore, the values were negative at positions D and F. To account for the results at positions A–C, it is necessary to assume that the vertical stress spreading range is important for the RD when ESF occurs and that the vertical stress spreading range is larger in the strong axial specification. This makes it easier for stress to reach the top end and causes earlier fracture of the strong axial specification. These results suggest that the stress spreading range of the strong

axial specification was larger vertically and smaller horizontally than that of the weak axial specification.

2.2.4 Standardized multiple regression analysis of characteristic values

To quantitatively verify how much each parameter had an influence on each characteristic value, SMRA was conducted.

The characteristic values with five explanatory variables are expressed in Eq. 1.

$$y = \sum_{i=1}^5 a_i x_i + \epsilon, \quad (1)$$

where y is the objective variable, x_i is the explanatory variable, a_i is its partial regression coefficient, and ϵ is the error.

Five explanatory variables were set as follows: dowel diameter d (mm), ratio of the pilot hole ph , ratio of the end distance to the diameter e , variable $side2$ that equals to 1 when the dowel position was D or E and 0 otherwise, and variable $side3$ that equals to 1 when the dowel position was F or G and 0 otherwise. Additionally, σ_{max} and σ_y were set as the objective variables. Each variable was standardized to have a mean of 0 and standard deviation of 1 using Eq. 2 before analysis.

$$\bar{p} = \frac{p - \mu}{\sigma}, \quad (2)$$

where p is the original value, \bar{p} is the standardized value, μ is the average value, and σ is the standard deviation. Supposing that the variable with the upper line indicates they have been standardized, Eq. 1 can be rewritten as in Eq. 3.

$$\bar{y} = \sum_{i=1}^5 a_i \bar{x}_i + \epsilon \quad (3)$$

The partial regression coefficients are representative of the influence degree of the parameter on the characteristic value. Therefore, this value can reveal the dominant influencing factor.

A comparison of the values of the partial regression coefficient is shown in Figure 11.

As shown in Figure 11, the overall results of σ_y and σ_{max} are roughly the same, but the degree of how the value is spread varies. Figure 11 indicates that ph had a stronger influence on σ_y than on σ_{max} . It also indicates that e , $side2$, and $side3$ had a stronger influence on σ_{max} than on σ_y . These results are consistent where the stress redistribution increased the stress spreading range at σ_{max} . Based on this assumption, the nailed damaged area was not small enough to ignore at σ_y , the stress spreading range widened at σ_{max} and the damaged area narrowed relatively. Similarly, even when the end or edge distance was narrow, it had no effect on σ_y because the stress spreading range at σ_y was also small. However, when the stress spreading range widened to some extent at σ_{max} , the range reached the edge and affected the strength. Consequently, the coefficients for σ_y and σ_{max} would differ. However, this cannot be confirmed only by these results.

An analysis of the a_e of σ_{max} suggests that e exerted the strongest influence on the σ_{max} of the PW and a stronger

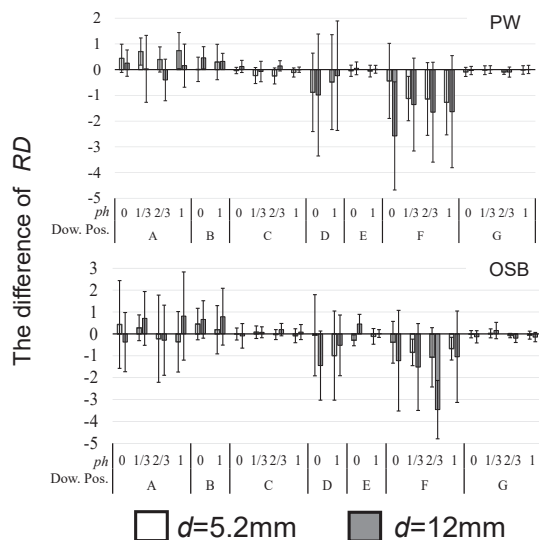


Figure 10: Comparison of RD differences between strong and weak axial specifications.

Note: Values of “strong axial specification - weak axial specification” are presented. Error bars indicate standard deviation.

influence on the σ_{\max} of the strong axial specifications than on their weak axial specifications. As described previously regarding the *RD*, the strong axial specification indicated a lower ductility than the weak axial specification when ESF occurred. This is assumedly attributable to the larger spread range of vertical stress in the strong axial specification. Based on this assumption, the σ_{\max} of the strong specification will certainly be affected by *e*.

Based on a comparison between $\overline{a_{side2}}$ and $\overline{a_{side3}}$, the overall trends were similar and the absolute value of $\overline{a_{side3}}$ was larger than that of $\overline{a_{side2}}$. Additionally, the values of $\overline{a_{side2}}$ and $\overline{a_{side3}}$ of σ_{\max} were strongly negative for PW-w and OSB-w. In general, a large stress spreads horizontally when a compressive stress is applied in the direction perpendicular to the grain, and the spreading of this stress contributes to the strength [8]. Therefore, it is natural that the weak axial specification was highly influenced by the edge distance.

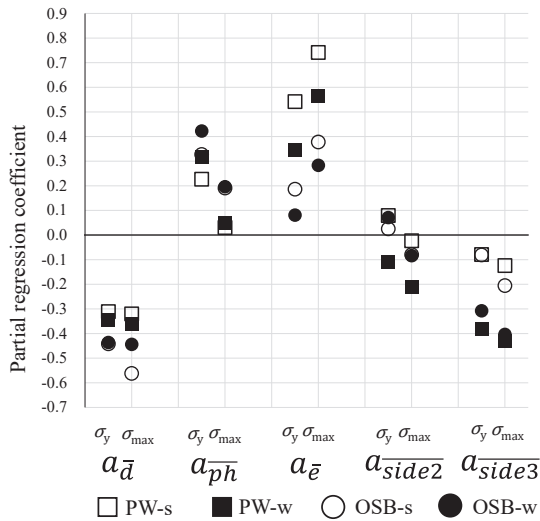


Figure 11: Comparison of partial regression coefficients.

3 STUDY BASED ON DETAILED OBSERVATION

3.1 MATERIAL AND METHOD

In this section, the process of stress spread, and fracture was clarified by utilizing DIC and CT scanning. Additionally, the assumptions suggested in the previous section: (1) PW and OSB is deformed dominantly in-plane and out-of-plane respectively; (2) the relative stress spread range is decreased with the larger diameter of the dowel; (3) the stress spread range is widened by load step; and (4) the bearing stress is spread vertically and horizontally in strong and weak specification respectively, also verified in this section.

Parameter was *d* (5.2 and 12mm) and material (PW-s,w and OSB-s,w). *ph* was configured as 1. Number of the specimen were two per a specification. The test setup was the same as in the previous section. Three test steps were set as shown in Figure 12 (1st step: 50% of the maximum load, 2nd step: maximum load, 3rd step: displacement equal to the diameter of the joint), and the force was

applied and removed each time. DIC was conducted during load process and CT scanning was conducted after unloaded. In the 1st step, the average value of the maximum load in the previous section was used as the predicted value, and when the load reached 50% of this value, the test was stopped, and the specimen was unloaded. In the 2nd step, when the load dropped 0.01 kN, the specimen was considered to have reached a certain maximum load and was unloaded. The test speed was 0.5mm/min for *d*=5.2mm and 1mm/min for *d*=12mm in the first and second step. In the third step, the test speed was twice.

For DIC procedure, random black dots on a white surface was painted on the face of the specimen. The surface image was captured at frequency of 0.2 Hz in the loading process.

In the CT scanning, specimens were scanned at 200 kV/200 μ A source output level, with no filters, scanning distance 962.5 mm to the specimen and 1400mm to the dictator, with 2000 angular projections (0.18 deg increments) and 0.75 second of exposure time per projection. The definition was 250 μ m/pixel.

3.2 RESULTS OF DIC TEST

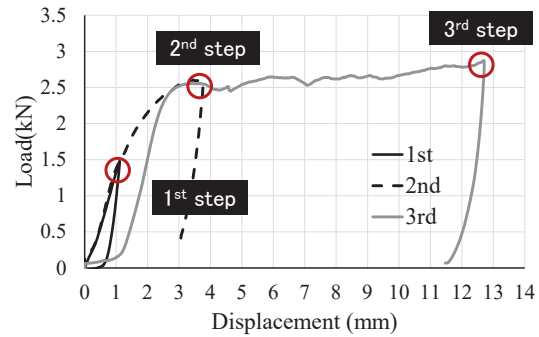


Figure 12: Schematic of three steps.

As shown in Figure 13, the *x*, *y* and shear strain distributions were obtained for five cross sections (load direction was regarded as *y* axis).

Figure 14 shows an example of the obtained strain distribution, which indicates that the strain is stronger in the central area than in other areas, and that some areas are not measured due to failure. We considered this area to be the local strain and fracture spread due to the bearing stress and measured the length of these areas by the following method. First, as shown in Figure 15, the mean μ and standard deviation σ of the

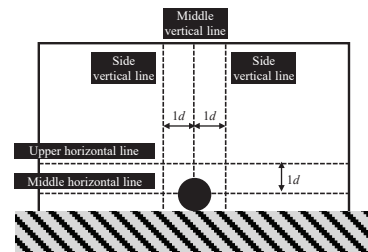


Figure 13: Measurement line of DIC.

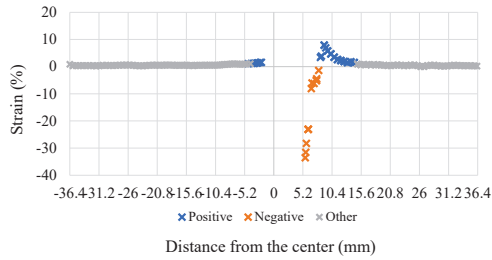


Figure 14: Example of strain distribution.
Note: material; PW-w, cross section; Middle horizontal line, diameter; 5.2mm, step; 3rd, strain; y.

strain in the range of 1~2 *d* from the left and right edges of the central horizontal section and the top of the central vertical section were calculated

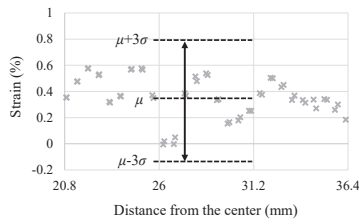


Figure 15: Variation of the values of strain near the edge of specimen.

based on the strain. Then, we calculated the range of strain that was not measurable due to fracture over the entire cross-section: failure, the range of strain higher than $\mu+3\sigma$: positive, and

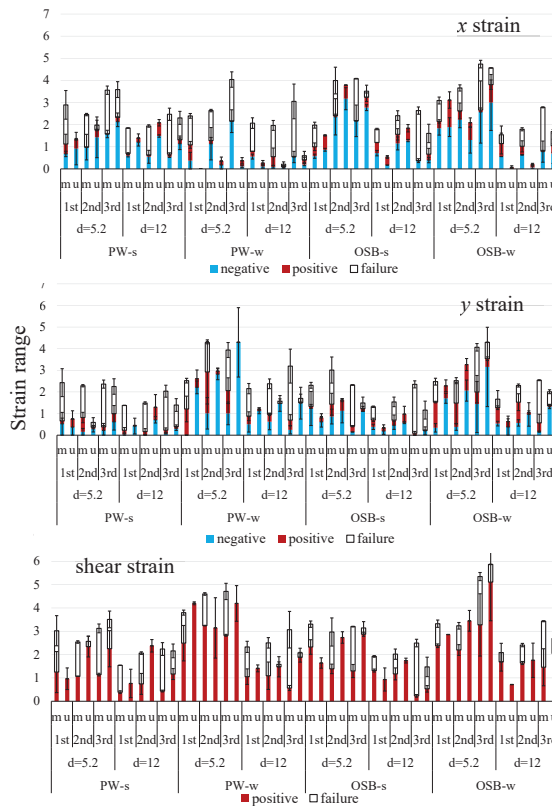


Figure 16: Comparison of strain range of horizontal cross section.
Note: “1st”, “2nd” and “3rd” indicate the test steps. “m” and “u” mean middle and upper horizontal cross section respectively.

the range of strain lower than $\mu-3\sigma$: negative. This process

was conducted for each strain direction, specimen, and step. The value obtained was divided by *d*, and the standardized value was defined as “strain range”.

Figure 16,17 shows comparison of strain ranges in the horizontal and vertical section respectively. The overall trend exhibited three distinct characteristics: I, the strain range was widened during each loading phase, particularly in the horizontal section; II, the relative strain range diminished with an increase in diameter; III, the strain range spread vertically and horizontally in the strong and weak axial specification respectively. The difference between strong and weak axial specification was more pronounced in PW. These results support the assumption referred in the previous section.

In PW-s, the range of vertical x-strain in the central and side sections exhibits positive and negative values, respectively. This outcome implies that the fiber was ruptured just above the dowel and concentrated on the lateral aspect of the dowel. This mechanism resulted in the compressive stress in the side section. The difference by *d* was smaller in PW-s than in any other panel type. The strain range was widened both horizontally and vertically during each loading phase.

The salient feature of the strain distribution in PW-w is that the y-strain spreads horizontally and extensively, akin to a stress distribution when timber is embedded laterally. The variation in *d* was substantial, which is likely attributed to the fact that the extent of spread is a fixed

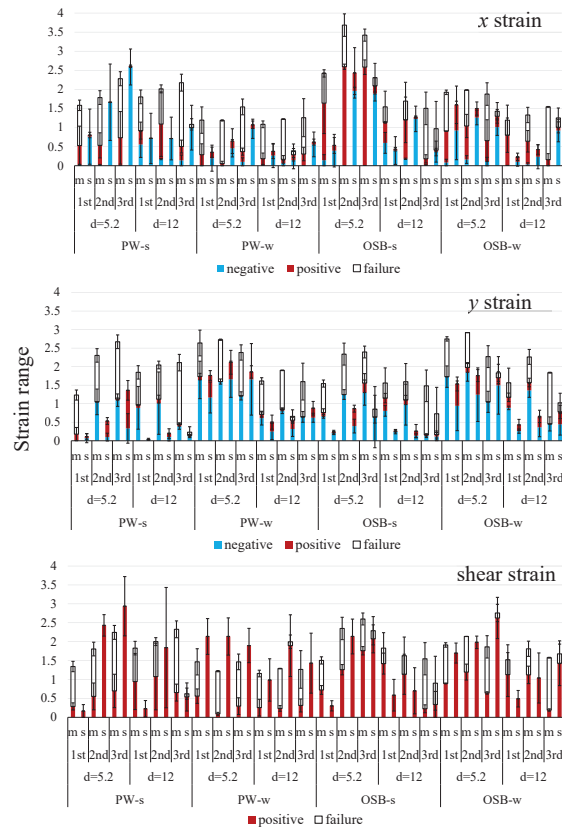


Figure 17: Comparison of strain range of vertical cross section.
Note: “1st”, “2nd” and “3rd” indicate the test steps. “m” and “s” mean middle and side vertical cross section respectively.

range, regardless of the pressure area, and in alignment

with prior research⁹). Although the strain range was broadened horizontally during each loading phase, this was not the case for the vertical angle, suggesting that the embedding depth remained unchanged by the step. The difference between strong and weak axial specification was pronounced more slightly in OSB than in PW. The variation in d was substantial. The strain range was broadened significantly only horizontally during each loading phase.

The shear strain in the horizontal section exhibited minimal expansion during each loading phase except horizontal section in OSB-s. Furthermore, the shear strain in the central vertical section was less pronounced than that in the peripheral section. As depicted in Figure 18, a graph of y strain and shear strain are superimposed in the upper horizontal section. The peak of shear strain was coincident with the base of the y strain peak. Thus, the range of shear strain can be considered to be situated at the periphery of the y strain range, and the length of this boundary did not expand, even as the range of y strain widened.

3.3 RESULTS OF CT SCANNING TEST

Internal cross-sectional images of five plywood layers and three OSB layers were acquired via CT scanning at the locations depicted in Figure 18. The brightness and contrast of each step were harmonized using the

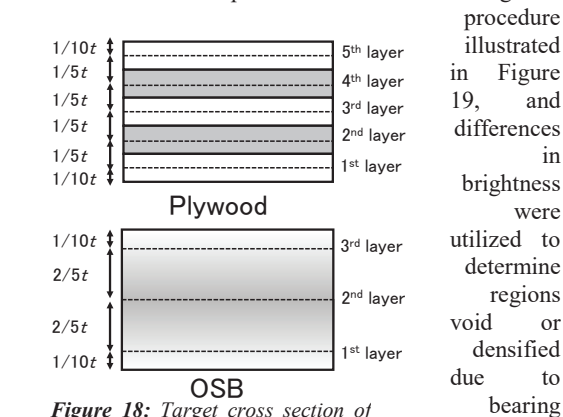


Figure 18: Target cross section of analysis.

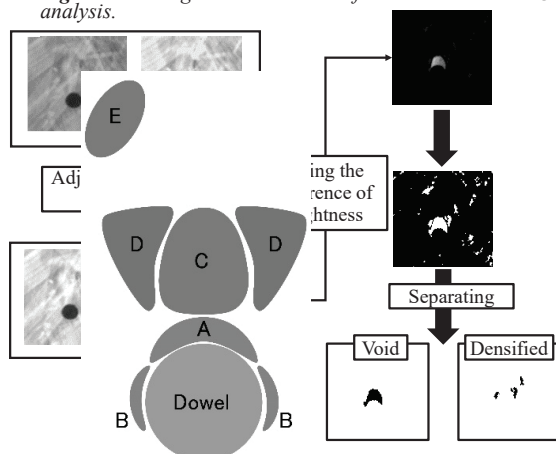


Figure 19: Overall method of analysing the change of the density. Figure 20: Classification of void or densified area.

difference images were obtained for the "1st step-2nd step (plasticity difference (PD))" and "2nd step-3rd step (ultimate difference (UD))" for each specimen and each cross-section.

For the derived difference images, the void and densified regions were categorized as A (immediately above to the dowel), B (left and right of the dowel), C (above the dowel), D (diagonally above the dowel), and E (otherwise), as depicted in Figure 20, to ascertain the location of the alteration for each specification, each layer, and each step. Based on this identification of fracture location, it was established whether the layer of varying specifications manifested identical forms of fracture or not. The concrete procedure is as follows.

Initially, an assessment was conducted to determine if the mode of failure varied contingent on the location of the target layer, either on the surface or inner layer.

Table 4: Comparison of R^2 values.

Comparison	Material	Step	R^2 value
Inner vs Outer	PW	PD	0.85
		UD	0.66
	OSB	PD	0.66
		UD	0.38
Strong vs Weak	PW	PD	0.61
		UD	0.24
	OSB	PD	0.55
		UD	0.53

In this regard, the first and fifth layers of plywood, and the first and third layers of OSB were deemed as surface layers, while the third layer of plywood and the second layer of OSB were deemed as inner layers. The likelihood of density changes occurring under each condition was evaluated, and a comparison list was generated and presented in Table 3. Subsequently, a regression analysis was performed on this list, yielding a graph as depicted in Figure 21, with the R^2 value serving as an indicator of similarity in fracture form between surface and inner layers when other conditions were matched. This analysis was separately conducted for plywood and OSB, and for PD and UD, resulting in four distinct R^2 values. A similar method was utilized to establish whether the failure modes differed between strong-axis and weak-axis layers.

Table 3: Schematic of list for comparison of failure behavior between outer and inner layer.

Direction	Diameter (mm)	Void or densified	Probability of change in density at ...	Outer Inner	
				Outer	Inner
Strong	5.2	void	A	1	1
			B	0.5	0.5
			C	0.5	1
			D	0	0
			E	0	0
Strong	12	densified	A	1	1
		
			A
Weak	5.2	void	A
		

The findings, presented in Table 4, demonstrate that for plywood, the impact of the layer's position on failure mode is negligible, whereas the variation in fiber direction accounts for the discrepancy in failure mode. Conversely, for OSB, the results indicate that the layer's position

significantly influenced the failure mode, particularly in the UD direction, and that the variance in fiber direction had no impact on the variation in failure mode. These results demonstrate the assumption referred in the previous section.

Moreover, the orientation of the fibers in the odd-numbered veneer layers in PW-s and the even-numbered veneer layers in PW-w (and vice versa) are identical. Consequently, a common method was employed to ascertain if the disparity in fracture form was due to the disparity between the odd- and even-numbered layers. The R^2 value was 0.82 for PD and 0.80 for UD, demonstrating that the mode of plywood failure is predicated on the direction of the veneer fibers, independent of the layer's arrangement.

Table 5 illustrates the probability of density fluctuation occurring in each specification. The occurrence of densification at position B was commonplace in the case of strong axial veneers in plywood, which may be attributed to the convergence of fibers on both sides of the dowel brought about by fiber dissociation in the center. At location C in the UD, void and densification also occurred, likely as a result of the upward propagation of cracks during large deformation. The weak axial veneer experienced void and densification at locations C and D in the UD, whereby the veneer was altered by bearing stress and undergoes plasticization and fracture above and to the right and left of the dowel, with the deformation failing to recover even upon unloading. The surface layer of OSB displays a plethora of void areas (B, C, D and E), presumably resulting from surface delamination. Only the inner layer of OSB experienced densification, with void and densification occurring frequently at location C. The fracture location of the inner layer can be characterized as intermediate between a strong-axis veneer and a weak-

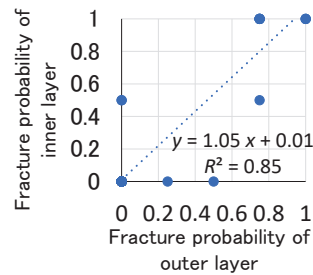


Figure 21: Examples of regression analysis of fracture probability.

axis veneer. These findings suggest that out-of-plane delamination is predominant in the surface layer, while in-plane compressive deformation is predominant in the inner layer.

The area of the difference image is divided by the area of the dowel and standardized for comparison in Figure 22. In PW, the weak axial veneer has a larger densified and void area than the strong axial veneer, and the difference in densification area is larger. This is because the convergence to the left and right due to fiber dissociation was an indirect deformation caused by a stress perpendicular to the direction of the applied force, while the embedment into the weak axial veneer is a direct deformation occurring parallel to the direction of the applied force. The densified area decreased with increasing diameter, but the void area did not change significantly with diameter. As mentioned above, it can be concluded that OSB causes delamination in the surface layer and compressive deformation in the inner layer. In addition, the standardized void area of the surface layer shows differences depending on the diameter, although the standard deviation is significant. In other words, the absolute value of the delamination area does not seem to vary with diameter.

4 CONCLUSIONS

The comprehensive testing of wood-based panels was performed to assess their bearing capacity. A systematic examination was carried out to discern the correlation between failure mode and parameters. By incorporating the remained distance, the interdependence between ductility and parameters was validated. Standardized multiple regression analysis of the characteristic values was also executed, yielding an understanding of the influence of various conditions on the values. These results provide insights into the failure behavior and stress distribution, supporting certain hypotheses.

A detailed investigation was performed using DIC and CT scanning techniques to shed light on the stress distribution and fracture processes. Three load steps were configured and subjected to cyclic loading. Verification and comparison were carried out for each specification, layer, and step, providing a clearer understanding of the stress distribution and fracture processes. These results are

Table 5: Comparison of probability of change in density at each area.

layer	d (mm)	step	Change in density	A	B	C	D	E		
Strong	5.2	PD	Void	0.9	0.2	0	0	0		
			Densified	0.9	0.6	0	0	0		
		UD	Void	1	0.4	0.8	0	0		
			Densified	1	0.9	0.6	0	0		
		12	PD	Void	1	0	0	0	0.1	
				Densified	1	0.1	0	0	0	
	UD		Void	1	0.4	0.7	0.2	0.3		
			Densified	1	0.5	0.5	0.1	0.1		
	Weak		5.2	PD	Void	0.8	0.3	0.2	0.2	0
					Densified	0.9	0	0	0	0
		UD		Void	1	0.3	1	0.9	0.3	
				Densified	0.9	0.2	1	0.7	0.1	
12		PD		Void	1	0	0	0	0	
				Densified	0.9	0.1	0	0	0	
		UD	Void	1	0.1	1	0.5	0.3		
			Densified	1	0.6	0.8	0.5	0.1		
		outer	5.2	PD	Void	1	0.125	0.375	0.25	0.125
					Densified	0.5	0.25	0	0.25	0.125
UD				Void	1	0.625	0.875	0.625	0.75	
				Densified	0.5	0.125	0.125	0.25	0.25	
12	PD			Void	1	0	0	0	0.125	
				Densified	0.375	0	0	0	0	
	UD		Void	1	0.25	1	0.75	0.75		
			Densified	0.125	0	0	0	0.25		
	5.2		PD	Void	1	0.25	0.5	0.25	0.25	
				Densified	0.75	0	0.25	0.25	0	
UD			Void	1	0.5	0.75	0.25	0.25		
			Densified	0.75	0	0.5	0.75	0		
12		PD	Void	1	0	0.25	0.25	0		
			Densified	1	0	0	0	0		
	UD	Void	0.75	0	0.75	0.5	0			
		Densified	0.75	0	0.5	0.25	0			

Note: left and right table shows results of plywood and OSB respectively.

consistent with the conclusions drawn from the comprehensive testing.

ACKNOWLEDGEMENT

Plywood was provided by SEIHOKU CORPORATION. I would like to thank you all those involved. This study was also supported by Grant-in-Aid for JSPS Research Fellow (no. 20J20611).

REFERENCES

- [1] K. Sawata, and M. Yasumura. Determination of embedding strength of wood for dowel-type fasteners. *J. Wood Sci.*, 48:138-146, (2002).
- [2] C. Sandaas, and A. K. Sarnaghi, and J. van de Kuilen. Numerical modelling of timber and timber joints: computational aspects. *Wood Sci. and Technol.*,54: 31-61, 2020.
- [3] N. Sekino, S. Morisaki. The Effects of Board Density and Board-Edge Distance of Nails on Lateral Nail-Resistance of Low-Density Particleboards. *Mokuzagakkaiishi*, 33(9):694-701(1987).
- [4] K. Ogawa, M. Harada, T. Shibusawa, and K. Miyamoto. Method for measuring the resistances produced on parallel and perpendicular veneers in plywood under nail embedment loading. *J. Wood Sci.*, 65(1) (2019).
- [5] Japanese Agricultural Standard (2003) JAS for plywood. Japanese Agricultural Standards Association, Tokyo.
- [6] Japanese Agricultural Standard (2013) JAS for OSB. Japanese Agricultural Standards Association, Tokyo.
- [7] JIS A 5508, "nails," Japanese standard association, 2009.
- [8] ASTM D1037-12 (2017) Standard test method for evaluating properties wood-based fiber and particle panel materials. ASTM International, West Conshohocken, PA.
- [9] A. J. M. Leijten. The bearing strength capacity perpendicular to grain norway spruce- Evaluation of three structural timber design models, *Const. and Buid. Mater.*, 105(15):528-525(2016).